DOI: 10.1002/ejic.200900617

Ferromagnetic Properties of a Trinuclear Nickel(II) Complex with a Trithiocyanurate Bridge

Pavel Kopel,[a] Jerzy Mrozinski,*[b] Karel Doležal,[c] Vratislav Langer,[d] Roman Boča,[e] Alina Bieńko,[b] and Andrzej Pochaba[b]

Keywords: Nickel / Magnetic properties / Bridging ligands / Multinuclear complexes

A novel trinuclear nickel(II) complex with *N*,*N*,*N*′,*N*′′,*N*′′-pentamethyldiethylenetriamine (pmdien) and a trithiocyanurate(3–) (ttc^{3-}) bridge of composition $[Ni_3(pmdien)_3(\mu\text{-}ttc)](ClO_4)_3$ (**1**) was prepared. The X-ray crystal structure of **1** was determined, revealing the tris-N,S chelating mode of the trithiocyanurate bridge, forming a regular triangular Ni^{II}_3 core. A deformed trigonal bipyramidal arrangement of the central atoms was further achieved by coordination of three pmdien N atoms. The complex shows a ferromagnetic exchange interaction among the Ni^{II} magnetic centers that is tuned by single-ion anisotropy and/or antisymmetric exchange. The complex orders ferromagnetically at T_c = 10 K and exhibits spin-glass properties.

Introduction

Transition-metal complexes containing bridges connecting central atoms have received considerable interest not only as bioinorganic model complexes and catalysts, but they are also studied for their interesting structural, magnetic, and spectral properties. The magnetic exchange interactions, antiferromagnetic or ferromagnetic, are of interest, as the complexes can find industrial applications.[1–3] From both structural and magnetic aspects, binuclear copper(II) complexes have been well studied and much fewer triangular trinuclear ones have been described. In the literature we can find examples of these trinuclear complexes where the copper centers are often bridged by hydroxy groups or nitrogen heterocycles.[4–6]

If we have in mind trinuclear nickel(II) complexes, we can find in the literature linear ones, for example, linear trinuclear nickel(II) complex with thiocyanato and pyridazine bridges have been reported by Cano et al.[7] $[\{Ni(dien)\}_2(\mu\text{-}ox)\{\mu\text{-}Ni(CN)_4\}]$ can serve as an example of a trinuclear complex with oxalato as well as cyano bridges, but from a magnetic point of view, the compound can be treated as a dimer.[8] More interesting are azido-bridged trinuclear triangular complexes $[\{Ni(tet)\}_3(\mu\text{-}N_3)_3](PF_6)_3$ and $[\{Ni(tet)\}_3(\mu\text{-}N_3)_3](ClO_4)_3$, tet = triethylenetetraamine with antiferromagnetic exchange interactions.[9] $[Ni_3(dtox)(dtoxH)_2](ClO_4)_2$ ($dtoxH_2$ = 4,7-dithiadecane-2,9-dione dioxime), $[\{Ni_3(medpt)_3(NCS)_4\}(\mu_3\text{-}CO_3)]$ [medpt = bis(3-aminopropyl)methylamine], and $[\{Ni_3(medpt)_3(NCSe)_4\}(\mu_3\text{-}CO_3)]$ are further examples of irregular triangular nickel(II) complexes, structurally characterized, showing weak and very strong antiferromagnetic interactions, respectively.[10–12] We can notice that in all the above-mentioned nickel(II) complexes, except for that containing the $Ni(CN)_4^{2-}$ unit, the central atoms are in a deformed octahedral arrangement.

As we are particularly interested in the study of trinuclear transition-metal complexes, we have focused our attention towards complexes with a 1,3,5-benzenetricarboxylato bridge, but it is well known that there is a very wide range of possible coordination modes of carboxylato groups, leading very often to the formation of polynuclear species. Moreover, the distance among the central atoms connected by the bridge is too big to propagate strong magnetic interactions. Trithiocyanuric acid ($ttcH_3$), also referred to as trimercaptotriazine, attracted our attention as well. Potentially six donor atoms can be employed for coordination to central atoms. In our previous papers we structurally characterized a series of mononuclear nickel(II) complexes with chelating N,S mode or N-only coordinated $ttcH^{2-}$ anion. To prevent formation of polymers with the anion, we used tetradentate, $[Ni(bapen)(ttcH)]\cdot 2H_2O$ [bapen = *N*,*N*′-bis(3-aminopropyl)ethylenediamine], [Ni(bappn)(ttcH)]·

[a] PPG Architectural Coatings EMEA, Primalex a.s., 33824 Břasy, Czech Republic
[b] Faculty of Chemistry, University of Wroclaw, 14 F. Joliot-Curie, 50383 Wroclaw, Poland
Fax: +48-713-757-307
E-mail: jmroz@wchuwr.chem.uni.wroc.pl
[c] Laboratory of Growth Regulators, Institute of Experimental Botany ASCR & Palacký University Šlechtitelů 11, 78371 Olomouc, Czech Republic
[d] Environmental Inorganic Chemistry, Department of Chemical and Biological Engineering, Chalmers University of Technology, 41296 Göteborg, Sweden
[e] Institute of Inorganic Chemistry, Technology and Materials, Slovak University of Technology 81237 Bratislava, Slovakia

$1.5H_2O$ [bappn = *N*,*N*′-bis(3-aminopropyl)-1,3-propanediamine], [Ni(taa)(ttcH)] [taa = tris-(2-aminoethyl)amine], and tridentate N-donor ligands [Ni(dpta)(ttcH)(H_2O)]·H_2O (dpta = dipropylenetriamine), [Ni(pmdien)(ttcH)].[13–17]

Next examples of different coordination modes of ttc can be found in the CCDC. Thus, the bridging, bischelating N,S mode occurs in [{Co$(en)_2$}$_2$(μ-ttc)]$(ClO_4)_3$·$2H_2O$ (en = ethylenediamine),[18] whereas complexes of composition [{Au(PPh_3)}$_3$(μ-ttc)], [{HgMe}$_3$(μ-ttc)], [{$SnMe_3$}$_3$(μ-ttc)], and [{$SnPh_3$}$_3$(μ-ttc)] are examples of trinuclear species, where ttc coordinates to S atoms only.[19–21] Quite recently, Kar et al. characterized a trinuclear ruthenium(II) complex of composition [{Ru$(L)_2$}$_3$(μ-ttc)]$(ClO_4)_3$ (L = phenylazopyridine), where the centers are bridged in a tris-N,S chelating mode of the ttc anion.[22]

We report herein, to the best of our knowledge, the first example of a trinuclear nickel(II) complex of ttc with a regular triangular Ni_3 core. The compound was characterized by elemental analysis and a combination of MAS, IR, and UV/Vis spectroscopy. X-ray crystallography unambiguously confirmed the bridging character of the ttc trianion and the coordination of three nitrogen atoms of pmdien to each central atom. Also, the absolute structure was established by X-ray diffraction by using the anomalous signal from both the Ni and S atoms. We further report results of magnetic measurements. It was revealed that, in **1**, ferromagnetic exchange interaction among nickel centers occurs. It was further tuned by asymmetric exchange and/or antisymmetric exchange.

Results and Discussion

Synthesis and Spectral Study

[Ni_3(pmdien)$_3$(μ-ttc)]$(ClO_4)_3$ (**1**) is readily prepared by reaction of nickel perchlorate, pmdien, and $ttcNa_3$ in ethanol or methanol in a 3:3:1 molar ratio. It is necessary to use perchlorate for the synthesis, as reactions of other nickel salts lead to the preparation of the mononuclear complex [Ni(pmdien)(ttcH)],[17] although various molar ratios and pH conditions were employed. Complex **1** is soluble in ethanol and can be recrystallized from warm methanol.

In addition to elemental analysis, mass spectrometry was used to characterize **1**. The ESI+ mass spectra display an intense peak at *m*/*z* = 869, corresponding to the trinuclear molecular ion of the composition [Ni_3(pmdien)$_3$(ttc)H]$^+$. There are also minor peaks at *m*/*z* = 969 and 1069, which can be attributed to ClO_4^- – aduced multiply protonated species [Ni_3(pmdien)$_3$(ttc)H_2]$^{2+}$ and [Ni_3(pmdien)$_3$(ttc)-H_3]$^{3+}$, respectively. The same adduct formation with the perchlorate ion was already reported for such types of complex ions.[10] The peaks observed at lower *m*/*z* = 699, 636, 232, 178, and 174 correspond to different fragments of the trimer and its organic parts.

There are broad bands in the IR spectrum of **1** with maxima at 2901 and 2976 cm^{-1} that can be connected with $\nu_s(CH_2)$ and $\nu_{as}(CH_2)$ vibrations, whereas a broad band with a maximum observed at 3408 cm^{-1} can be attributed to ν(C–H) and ν(N–H) vibrations.[23] The bands attributable to vibrations of uncoordinated perchlorate groups are observed at 627, 934, and 1040 cm^{-1}. The peaks connected with ν(C–N) vibrations of the triazine ring appear at 1235 and 1631 cm^{-1}, whereas a peak that belongs to the ν(C–S) vibration of the ttc anion appears at 879 cm^{-1}. These assignments are in good agreement with calculated infrared frequencies for the ttc anions.[24]

For high-spin trigonal bipyramidal nickel complex the bands found, in diffuse-reflectance spectrum, at 9600 and 15100 cm^{-1} can be probably assigned to $^3E' \rightarrow {}^3E''$ and $^3E' \rightarrow {}^3A_2'$ d–d transitions, respectively.[25,26] The band at 29600 cm^{-1} in the near UV region can be connected with a metal-to-ligand charge-transfer (MLCT) transition.

Molecular Structure

The numbering scheme of the Ni complex is shown in Figure 1. Selected bond lengths and angles are listed in Table 1, whereas the crystallographic and refinement data are summarized in Table 2.

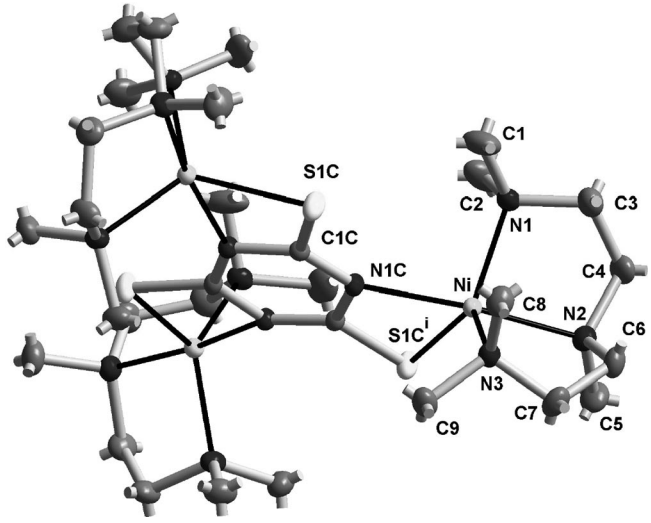

Figure 1. Numbering scheme of the Ni complex with atomic displacement ellipsoids drawn at 30% probability level. Hydrogen atoms are omitted for clarity.

The crystal structure of **1** is formed by a complex cation and three perchlorate anions. The trithiocyanurate trianion forms a bridge among the three central nickel atoms. The Ni–Ni distance is 5.9910(5) Å. In the trinuclear complex, all three sets of S,N donor atoms of the bridging ttc trianion are used for coordination to the central atoms. The nickel atoms are pentacoordinate, and the geometry can be best described as deformed trigonal bipyramid (TBP) formed by three N atoms of pmdien and a chelating N,S set of the ttc anion. In the basal plane of the TBP, there are two terminal N atoms of pmdien and an S atom of ttc, whereas the apical positions are occupied by a central N atom of pmdien and an N atom of the ttc ring (Figure 2).

Table 1. Selected bond lengths and angles for **1**.[a]

Bond lengths [Å]			
Ni–N1	2.085(3)	Ni–S1Ci	2.3821(9)
Ni–N3	2.090(3)	S1C–C1C	1.719(3)
Ni–N2	2.140(3)	N1C–C1C	1.343(4)
Ni–N1C	2.174(3)	N1C–C1Ci	1.357(4)
Bond angles [°]			
N1–Ni–N3	120.13(13)	N2–Ni–N1C	171.21(11)
N1–Ni–N2	85.12(12)	N1–Ni–S1Ci	115.48(9)
N3–Ni–N2	85.41(12)	N3–Ni–S1Ci	124.32(9)
N1–Ni–N1C	98.31(11)	N2–Ni–S1Ci	102.18(9)
N3–Ni–N1C	99.67(11)	N1C–Ni–S1Ci	69.03(7)

[a] Symmetry transformations used to generate equivalent atoms: (i): $-z + 2$, $x - 1/2$, $-y + 3/2$.

We have already reported a structure of the mononuclear Ni^{II} complex [Ni(pmdien)(ttcH)],[17] where the nickel atom is also pentacoordinate with Ni–N bond lengths in the range 2.074–2.100 Å and a Ni–S distance of 2.3392(13) Å. In comparison with this structure, the Ni–N bond lengths (in **1**) in the apical positions [2.174(3) Å] are longer, as is the Ni–S1C bond length [2.3821(9) Å]. When we compare bond angles in both structures, we can conclude that the geometry about the nickel atom (in **1**) is closer to a regular TBP with equatorial angles of 120.13(13), 115.48(9), and 124.32(13)° (close to the regular angle 120°) and axial angle of 171.21(11)°, whereas the geometry of the nickel atom in [Ni(pmdien)(ttcH)] is rather an intermediate between TBP and square pyramid (SP) with equatorial angles of 143.55(14), 108.66(11), and 107.64(11)° and axial angle of 174.05(14)°. When we use the parameter τ,[27] defined as $\tau = (\theta - \Phi)/60$, where θ and Φ are two basal angles ($\theta > \Phi$) and $\tau = 1$ is for a regular TBP and $\tau = 0$ for SP geometry, the calculated values are $\tau = 0.78$ and $\tau = 0.51$ for **1** and [Ni(pmdien)(ttcH)], respectively (Figure 3).

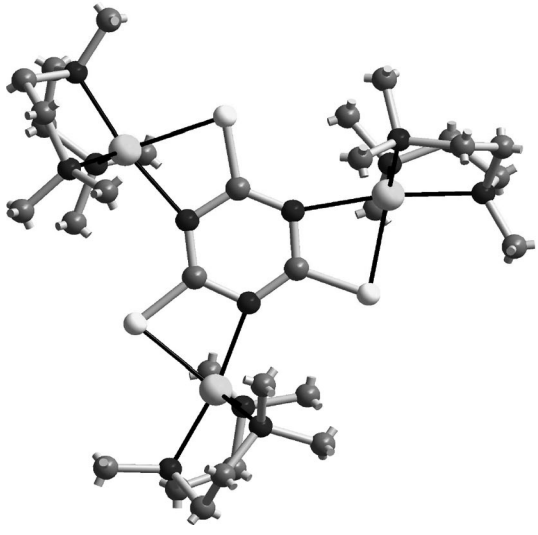

Figure 2. The Ni complex in projection along the crystallographic threefold axis.

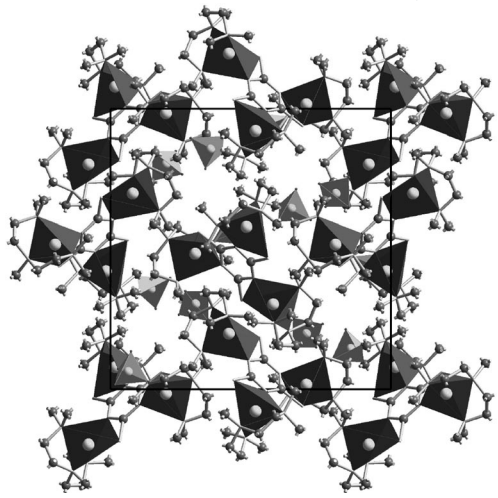

Figure 3. Contents of the unit cell in a view along the *a* axis. Ni polyhedra are in dark gray and the tetrahedra of the perchlorates are in light gray.

The only known structurally characterized trinuclear complex with trischelating bridging ttc($^{3-}$) is [{Ru(L)$_2$}$_3$-(ttc)](ClO$_4$)$_3$ (L = phenylazopyridine).[22] The ttc($^{3-}$) ligand is bonded to three ruthenium centers using all three avail-

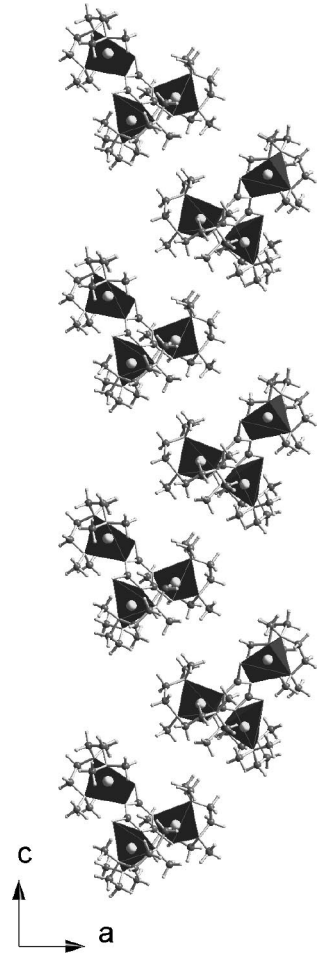

Figure 4. Right-handed helical arrangements of Ni complexes.

able N,S donor sets. Distorted octahedral surrounding about Ru atoms is completed by two phenylazopyridine units bonded in a bidentate manner. The Ru–N(ttc) distances are in the 2.088–2.122 Å range and the average Ru–S distance is 2.434 Å. In comparison with structure **1**, the Ru–N(ttc) distances are shorter, whereas the Ru–S distances are longer. The absolute structure determination of **1** revealed that there are right-handed helical arrangements of Ni complexes around the three mutually perpendicular (but not intersecting) screw axes. Thus, crystallization of **1**, even though there are no chiral moieties, results in the self-resolution of a pure homochiral network (see Figure 4). The shortest intermolecular distances between the metallic centers in the neighboring trimer unit are 8.701 and 8.853 Å.

Magnetic Properties

The temperature variation in the magnetization taken at low magnetic field (B = 0.5 T) was converted into the mean magnetic susceptibility, then corrected to underlying diamagnetism and used in calculating the product function $\chi T/C_0$ (dimensionless), where $C_0 = N_A\mu_0\mu_B^2/k_B$ is the reduced Curie constant (Figure 5).

At room temperature, $\chi T/C_0$ = 11.7, but this value starts to slightly decrease upon cooling to T = 70 K, at which point $\chi T/C_0$ = 11.2. Such a feature reflects some temperature-independent paramagnetism (TIP). Upon further cooling, this function increases and passes through a maximum at T = 16 K, where $\chi T/C_0$ = 14.3. This feature confirms a ferromagnetic exchange coupling among Ni^{II} centers.

The susceptibility data above 14 K were used for a preliminary determination of TIP = 13×10^{-9} m^3 mol^{-1} and J_0/hc = 2.5 cm^{-1} using the isotropic exchange model [Equation (1)].

$$\hat{H}^{iso}(a) = -J_0\hbar^{-2}[(\vec{S}_1\cdot\vec{S}_2)+(\vec{S}_1\cdot\vec{S}_3)+(\vec{S}_2\cdot\vec{S}_3)] + g\mu_B B_a\hbar^{-1}(\hat{S}_{1,a}+\hat{S}_{2,a}+\hat{S}_{3,a}) \quad (1)$$

In this model, the ground state is S = 3, and the remaining states are two S = 2 (J_0 above), three S = 1 ($3J_0$ above the ground state), and a singlet S = 0 ($6J_0$ above the ground state). This model does not reproduce the low-temperature susceptibility data, as with S = 3 ground state the effective magnetic moment should converge to a plateau of $\chi T/C_0$ = 16.0 (when all g = 2.0). The model also fails in reproducing the magnetization data: the observed magnetization per particle at B = 5 T and T = 2.0 K is only M_{mol}/N_A = 3.56 μ_B, which deviates heavily from the Brillouin function value of M_{mol}/N_A = 6.0 μ_B (when all g = 2.0). Attempts to improve the isotropic model by the molecular-field correction failed as well.

The involvement of the nonisotropic exchange evokes a number of nontrivial questions that can be answered only by a detailed numerical treatment. They are as follows: (i) Does the magnetic anisotropy originate only in the single ion anisotropy (D_{AA} parameter), or does the asymmetric exchange term (D_{AB} parameter) also contribute? (ii) Is it possible to apply a simplified model of the strong exchange coupling, or need a more general weak exchange limit be involved? (iii) Can the sign of the D parameters be fixed unambiguously? (iv) Is the asymmetric exchange the only source of zero-field splitting (ZFS), or does the antisymmetric exchange apply or even interfere?

In fitting the magnetic data a combined functional [Equation (2)] was minimized by utilizing a genetic algorithm of the nonlinear optimization.[28]

$$F = w_1\sum_{i=1}^{N}(\mu_{eff,i}^{c}-\mu_{eff,i}^{o})^2 + w_2\sum_{j=1}^{M}(M_j^{c}-M_j^{o})^2 \quad (2)$$

Because the J_0 value is rather low and because the expected magnetic anisotropy parameter for Ni^{II} centers is much higher (of the order of 10 cm^{-1}), the hypothesis of the strong exchange coupling limit, $|J_0|>>|D|$, is not fulfilled. Therefore, the matrix elements of the spin Hamiltonian were calculated in the basis set of uncoupled spins.[29]

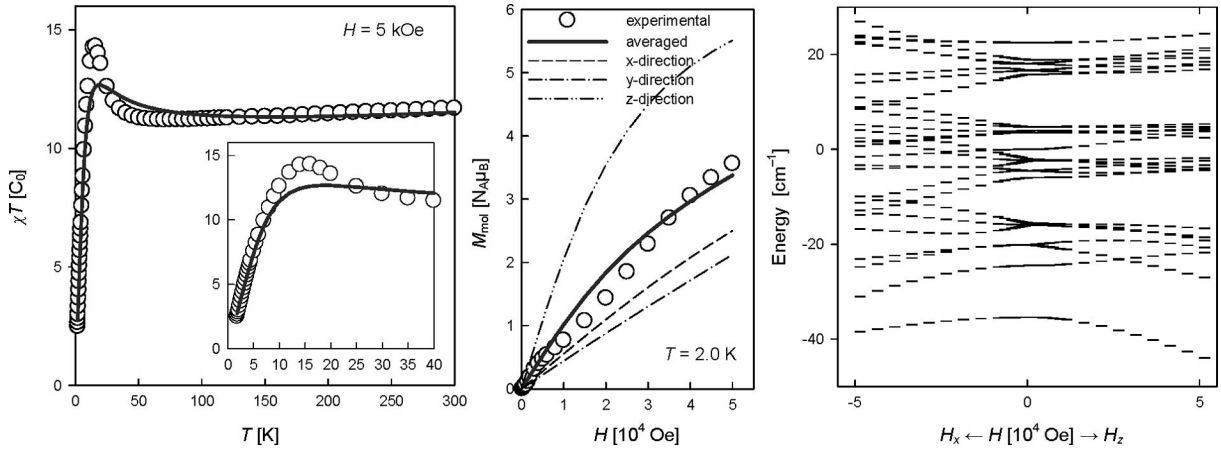

Figure 5. Product function (left), magnetization (center), and energy levels (right) for **1**. Filled points and solid lines represent fitted data with the anisotropy model (exclusively the single-ion anisotropy); model-1.

The single ion anisotropy was included by the generalized anisotropy Hamiltonian that accounts for all Cartesian elements of the spin–spin interaction tensor according to Equation (3).

$$\hat{H}^{\text{asym}}(a) = \hat{H}^{\text{iso}}(a) + \hbar^{-2}\sum_{A=1}^{3}\sum_{\alpha}^{x,y,z}\sum_{\beta}^{x,y,z} D^{A}_{\alpha,\beta}(\hat{S}_{A,\alpha}\hat{S}_{A,\beta}) \quad (3)$$

The elements of the molecular-frame $D[a]^{A}_{\alpha,\beta}$ tensor are made from a single D parameter referring to the local z axis of the individual center [Equation (4)].

$$\mathbf{D}^{A} = \mathbf{R}_{\varphi}\mathbf{R}_{\vartheta}\begin{pmatrix} -D/3 & 0 & 0 \\ 0 & -D/3 & 0 \\ 0 & 0 & 2/3D \end{pmatrix}(\mathbf{R}_{\varphi}\mathbf{R}_{\vartheta})^{-1} \quad (4)$$

where $\mathbf{R}_{\vartheta}$ and $\mathbf{R}_{\phi}$ are the rotation matrices that bring the local frame to the molecular one. In the present case of a triangulo-Ni_3 unit, the molecular z axis is parallel to the plane and thus the polar angles for individual atoms are ϑ_A = 90, 90, and 90°, and ϕ_A = 0, 120, and 240°, respectively. With such a setting the local z axis (threefold axis of an idealized trigonal bipyramid) points to the center of the triangle in analogy to recently reported systems.[38] In general, the matrix elements of the bilinear spin operators $\langle\cdots S_i' M_i'\cdots|\hat{S}_{A,\alpha}\hat{S}_{A,\beta}|\cdots S_i M_i\cdots\rangle$ form complex hermitian matrices.

The fitting procedure gave the following set of magnetic parameters for the anisotropy model: J/hc = 3.31 cm^{-1}, g = 2.40, D_{Ni}/hc = 17.1 cm^{-1} (χ_{TIP} – fixed). The discrepancy factor for susceptibility is R_1 = 0.055 and that for the magnetization is R_2 = 0.107. The agreement with the experimental data is satisfactory, although not perfect.

The most important message is the very high magnetic anisotropy reflected into high-positive value of D_{Ni}. With the value of J being small and that of D_{Ni} being high, the spin no longer is a good quantum number. Therefore, the energy levels cannot be identified as J multiplets additionally split by D parameters into Kramers doublets (e.g., $|M_s = \pm 3\rangle$, $|M_s = \pm 2\rangle$ and $|M_s = \pm 1\rangle$ lying at 9D, 4D, and D above the ground state $|M_s = 0\rangle$). On the contrary, we have the energy levels as shown in Figure 5. A test for the sign reversal of D_{Ni} was always wrong, so that the positive sign is fixed satisfactorily in the present case.

The symmetry of the chromophore for individual pentacoordinate Ni^{II} centers is somewhere between C_{4v} and D_{3h}. Therefore, the retrieved ZFS D parameter cannot be compared with data reported for hexacoordinate Ni^{II} complexes possessing D_{4h} or D_{2h} symmetry.[30,31]

The second model accounts for antisymmetric exchange [Equation (5)].

$$\hat{H}^{\text{anti}}(a) = \hat{H}^{\text{iso}}(a) + d_z\hbar^{-2}[(\vec{S}_1\times\vec{S}_2) + (\vec{S}_2\times\vec{S}_3) + (\vec{S}_3\times\vec{S}_1)]_z \quad (5)$$

The symmetry rules reveal that only the z component of the parameter vector will apply so that we are left with a single antisymmetric exchange parameter d_z. The net effect of the antisymmetric exchange is a kind of ZFS (different from that produced by the asymmetric exchange) and a marked drop in $g_x << 2$.

The set of magnetic parameters for model-2 is: J/hc = 1.67 cm^{-1}, g_z = 2.099, g_x = 1.265, d_z/hc = 4.95 cm^{-1}. This set reproduces the magnetization data much better (R_1 = 0.115, R_2 = 0.082; Figure 6). As before, the calculated energy levels and magnetization components show considerable anisotropy.

Below 14 K, the value of $\chi T/C_o$ decreases due to the combined effect of ZFS, saturation and/or intermolecular antiferromagnetic couplings. In this procedure, a Weiss constant was used to account for intermolecular interactions. The obtained rather small value of θ = –2.06 K in comparison to the large value of the D_{Ni} parameter indicates a dominant ZFS effect within the S = 1 local ground states of each Ni^{II} ion.

The occurrence of a magnetic phase transition was established by measuring the magnetization as a function of the temperature under a weak magnetic field. The field-cooled magnetization (FCM) and zero field-cooled magnetization (ZFCM) curves at 25 and 50 Oe are represented in Figure 7.

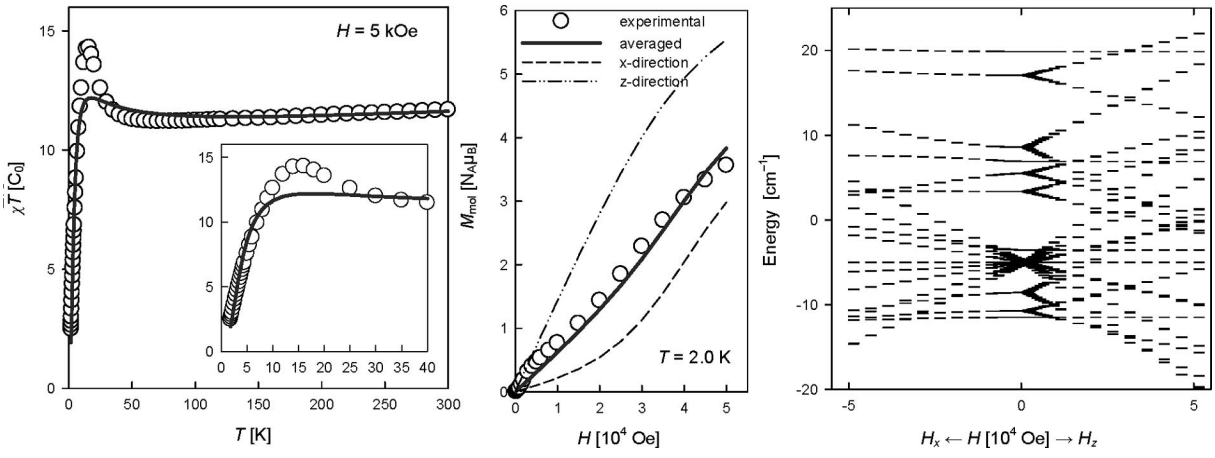

Figure 6. Effective magnetic moment (left), magnetization (center), and energy levels (right) for **1**. Filled points and solid lines represent fitted data with the antisymmetric exchange; model-2.

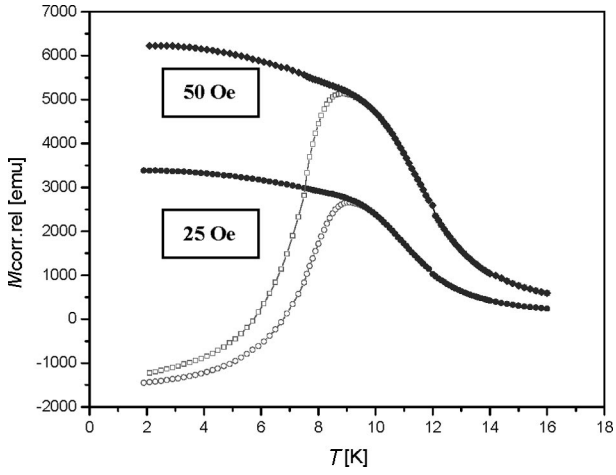

Figure 7. Temperature dependence of magnetization for **1** in the 16–2 K range and a field of 50 and 25 Oe, respectively: ■,● represent FCM; □,○ represent ZFCM.

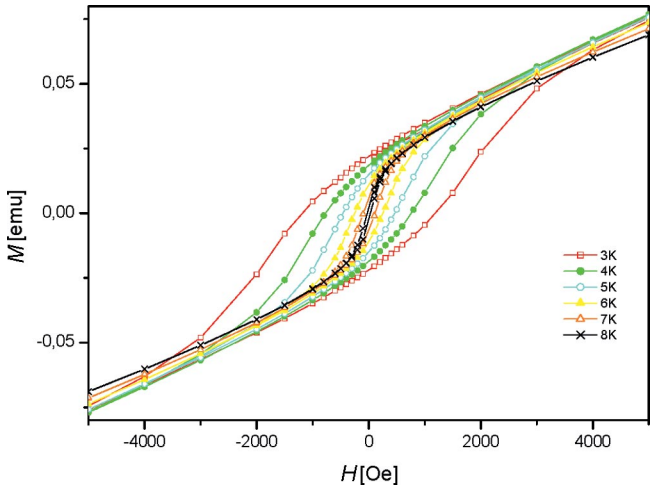

Figure 9. Hysteresis loops for **1** at variable temperature.

The FCM curve was obtained by cooling the sample from 16 to 2 K; it shows typical features of a ferromagnetic transition, that is, a rapid increase in M when T decreases below T_c = 10 K. When the field is increased, the ferromagnetic transition becomes less abrupt. The ZFCM curve was obtained by cooling down to 2 K in the zero field, then applying the field, and heating. At a given temperature below T_c, the ZFCM is smaller than the FCM, due to the fact that in this temperature range the applied field is too weak to move the domain walls. The ZFCM exhibits a maximum slightly below T_c as expected for a polycrystalline ferromagnet.[32]

The magnetic hysteresis at 2 K is shown in Figure 8. At this temperature, the remnant magnetization equals 4500 Oe and the coercive field is about 1250 Oe.

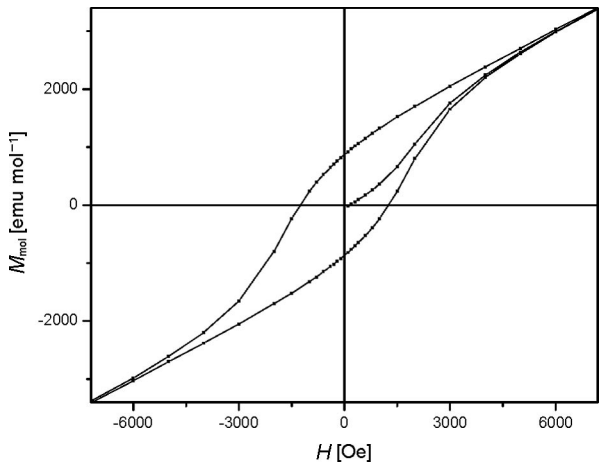

Figure 8. Hysteresis loop including the virgin curve for **1** at 2 K.

The development of the hysteresis loop upon heating (Figure 9) shows a lowering of the area of the hysteresis loop with increasing the temperature and going to zero about 8.1 K.

The AC magnetic susceptibility data collected for complex **1** in a zero-applied DC field results in relaxation of the magnetization. As the frequency of the oscillation increases, a lag in the in-phase component of the molar AC susceptibility, χ', is observed at low temperatures (Figure 10). The corresponding rise in the out-of-phase susceptibility χ'' is shown for switching frequencies, in each case χ'' achieves maximum (Figure 11). As the frequency of the AC field increases, the maxima of both χ' and χ'' are shifted towards higher temperatures.

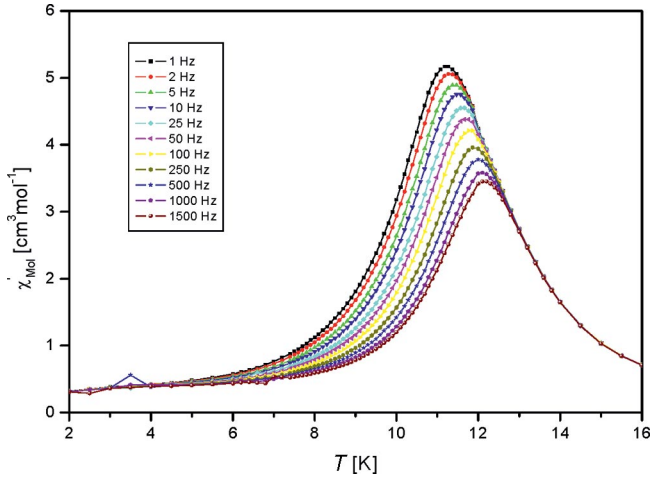

Figure 10. In-phase molar magnetic susceptibility for **1**.

Relaxation times follow on the Arrhenius relationship $\tau = \tau_o \exp(\Delta_{eff}/kT)$. Accordingly, a plot of $\ln\tau$ vs. $1/T$ is linear with a least-squares fit yielding pre-exponential factor $\tau_o = 8.8 \times 10^{-34}$ s and the effective energy barrier Δ_{eff} = 540 cm^{-1}. The observed value of the blocking temperature equals T_B = 10.2 K. The AC data shows a behavior that is not compatible with an SMM (single molecular magnet), whereas it may be appropriate for a spin-glass system.[39–41]

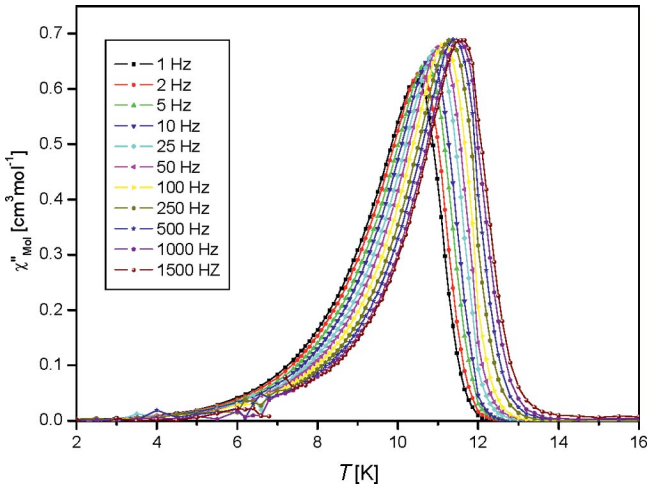

Figure 11. Out-of-phase molar magnetic susceptibility for **1**.

It seems interesting to compare the magnetic behavior of complex **1** with those obtained for the $[Cu_3(pmdien)_3(\mu\text{-}ttc)](ClO_4)_3$ trimer.[33] Both complexes contain the same bridging ligand and terminal ions but different M^{II} ions. The substitution of the Cu^{II} ion for the Ni^{II} ion causes a change in the nature of the magnetic interaction from antiferromagentic to ferromagnetic coupling.

This antiferromagnetic exchange coupling inside the trinuclear copper(II) unit is explicable by comparison to the related compound $[(talen)Cu^{II}_3]_n$[34] as well as in terms of the commonly accepted notion that the overlap of the magnetic orbitals favor antiferromagnetic coupling, whereas orthogonality of the magnetic orbitals and spin polarization mechanism lead to ferromagnetic coupling.

Conclusions

Compound **1** is the first example of a trinuclear nickel(II) complex of ttc with a regular triangulo-Ni_3 core, where each metal center is pentacoordinate. The magnetic data reveal a ferromagnetic exchange coupling among the Ni^{II} centers that is further tuned by asymmetric and/or antisymmetric exchange. The occurrence of a magnetic phase transition was established by measuring the FCM and ZFCM as a function of temperature under a weak magnetic field. Ferromagnetic coupling was confirmed by the magnetization measurements at 2, 3, 4, 5, 6, 7, and 8 K, where the hysteresis loop is well visible. The AC susceptibility data shows behavior that is compatible with a spin-glass system.

Experimental Section

General Remarks: All chemicals and solvents were supplied from Aldrich and Lachema (Czech Republic) and were used as received. C, H, N, and S analyses were carried out with an EA 1108 instrument (FISONS). IR spectra (400–4000 cm^{-1}) were recorded with an FTIR Spectrometer Spectrum One (Perkin–Elmer) by using KBr pellets, and diffuse-reflectance spectra (9000–35000 cm^{-1}) were obtained with a UV/Vis Spectrometer Lambda 35 (Perkin–Elmer) by using KBr pellets. The magnetization measurements of the powdered sample were accomplished over the temperature range 1.8–300 K by using a Quantum Design SQUID–based MPMSXL–5-type magnetometer at magnetic field 0.5 T and in the range 0–5 T at 2 K. The SQUID magnetometer was calibrated with the palladium rod sample. Corrections are based on subtracting the sample-holder signal and contribution χ_D estimated from the Pascal constants and equal 698×10^{-6} $cm^3\,mol^{-1}$. The AC measurements on a polycrystalline sample of the complex were performed at frequencies ranging from 1 to 1500 Hz with an AC field drive amplitude of 1 Oe and zero-field DC applied. The ESI+ mass spectra were recorded with a Waters ZMD 2000 mass spectrometer. The mass-monitoring interval was m/z = 10–1500. The spectra were collected by using 3.0 s cyclical scans and applying the sample cone voltages 20, 30, or 40 V, at the source block temperature 80 °C, desolvation temperature 150 °C, and desolvation gas flow rate 200 $L\,h^{-1}$. The mass spectrometer was directly coupled to a MassLynx data system. All m/z interpretations are based on ^{35}Cl and ^{58}Ni, respectively.

Caution! Perchlorate salts of metal complexes with organic ligands are potentially explosive. Only small amounts of these materials should be handled with great caution.

$[Ni_3(pmdien)_3(\mu\text{-}ttc)](ClO_4)_3$ (1): Pmdien (0.2 mL, 1 mmol) was added to a solution of $Ni(ClO_4)_2{\cdot}6H_2O$ (0.37 g, 1 mmol) in EtOH (50 mL). A solution of $ttcNa_3{\cdot}9H_2O$ (0.14 g, 0.33 mmol) in water (2 mL) was added to the reaction mixture with stirring. Green microcrystals started to appear during the addition. The reaction mixture was stirred for 1 h. The green product was separated by filtration, washed with small amounts of EtOH, and dried in air. Crystals suitable for X-ray analysis were obtained by very slow evaporation of the filtrate for a month. Yield: 268 mg, 68%. $C_{30}H_{69}Cl_3N_{12}Ni_3O_{12}S_3$ (1168.62): calcd. C 30.8, H 6.0, N 14.4, S 8.2; found C 30.2, H 5.8, N 13.9, S 7.8. IR (KBr): $\tilde{\nu}$ = 462 (w), 493 (m), 583 (w), 627 (s), 751 (w), 767 (m), 777 (m), 803 (s), 879 (s), 915 (m), 934 (s), 987 (m), 1040 (s), 1178 (w), 1235 (s), 1286 (m), 1301 (w), 1458 (s), 1631 (m), 1865 (w), 2018 (m), 2110 (w), 2169 (w), 2403 (w), 2814 (w), 2901 (s), 2976 (s), 3408 (s) cm^{-1}. UV/Vis: λ = 9600, 15100, 29600 nm. MS (ESI+): m/z = 1069, 969, 869 $[Ni_3(pmdien)_3(ttc)H]^+$, 699 $[Ni_3(pmdien)_3H]^+$, 636 $[Ni_2(pmdien)_3\text{-}H]^+$, 232 $[Ni(pmdien)H]^+$, 178 $[ttcH]^+$, 174 $[pmdienH]^+$.

X-ray Crystallographic Study: Diffraction data were collected by using a Siemens SMART CCD diffractometer with Mo-K_α radiation (λ = 0.71073 Å, graphite monochromator). The crystals were cooled to 173(2) K by a flow of nitrogen gas by using the LT-2A device. A full sphere of reciprocal space was scanned by 0.3 steps in ω with a crystal-to-detector distance of 3.97 cm. Preliminary orientation matrix was obtained from the first frames by using SMART.[35] The collected frames were integrated by using the preliminary orientation matrix, which was updated every 100 frames. Final cell parameters were obtained by refinement of the positions of reflections with $I > 10\sigma(I)$ after integration of all the frames by using SAINT software.[35] The data were empirically corrected for absorption and other effects by using the SADABS program.[36] The structures were solved by direct methods and refined by full-matrix least-squares on all $|F^2|$ data by using SHELXTL software.[37] Selected bond lengths and their estimated standard deviations are listed in Table 1. The crystallographic and refinement data are summarized in Table 2.The molecular graphics were prepared by using the DIAMOND program.[38] CCDC-637068 (for **1**) contains the supplementary crystallographic data for this paper. These data can be obtained free of charge from The Cambridge Crystallographic Data Centre via www.ccdc.cam.ac.uk/data_request/cif.

Table 2. Crystal data and structure refinement for **1**.

Empirical formula	$C_{30}H_{69}Cl_3N_{12}Ni_3O_{12}S_3$
Formula weight	1168.62
Temperature [K]	173(2)
Wavelength [Å]	0.71073
Crystal system	cubic
Space group	$P2_13$
a [Å]	17.3804(3)
b [Å]	17.3804(3)
c [Å]	17.3804(3)
Volume [Å^3]	5250.24(16)
Z	12
$D_{calcd.}$ [Mg m^{-3}]	1.478
Absorption coefficient [mm^{-1}]	1.398
F(000)	2448
Crystal size [mm]	0.38 × 0.17 × 0.11
θ range for data collection [°]	1.66 to 30.66
Index ranges	$-24 \le h \le 24$ $-24 \le k \le 24$ $-24 \le l \le 24$
Reflections collected	85826
Independent reflections	5445 (R_{int} = 0.0551)
Completeness to θ = 30.66° [%]	100.0
Absorption correction	multiscan
Max. and min. transmission	0.8614 and 0.6186
Refinement method	full-matrix least squares on F^2
Data/restraints/parameters	5445/0/197
Goodness-of-fit on F^2	1.010
Final *R* indices [$I > 2\sigma(I)$]	R_1 = 0.0378, *wR*2 = 0.1067
R indices (all data)	R_1 = 0.0528, *wR*2 = 0.1243
Absolute structure parameter	–0.090(16)
Largest diff. peak and hole [e Å^{-3}]	1.042 and –0.404

Acknowledgments

Professor Dante Gatteschi (University of Florence) is thanked for valuable discussions. The 6th Framework Programme EU [NoE - "Molecular Approach to Nanomagnets and Multifunctional Materials (MAGMANet)], Ministry of Science of the Czech Republic (grant MSM6198959216), and Grant Agency of Slovakia (grants VVCE-0004-07, APVV-0007-07, VEGA 1/0213/08, COST-0006-06) are acknowledged for the financial support.

[1] D. Gatteschi, O. Kahn, R. D. Willet, *Magneto-Structural Correlations in Exchange Coupled Systems*, Reidel, Dordrecht, **1984**.
[2] O. Kahn, *Molecular Magnetism*, VCH, New York, **1993**.
[3] J. Mrozinski, *Coord. Chem. Rev.* **2005**, *249*, 2534.
[4] S. Ferrer, J. G. Haasnoot, J. Reedijk, E. Muller, M. B. Cingi, M. Lanfranchi, A. M. M. Lanfredi, J. Ribas, *Inorg. Chem.* **2000**, *39*, 1859.
[5] S. Ferrer, F. Lloret, I. Bertomeu, G. Alzuet, J. Borras, S. Garcia-Granda, M. Liu-Gonzalez, J. G. Haasnoot, *Inorg. Chem.* **2002**, *41*, 5821.
[6] L. M. Mirica, T. D. P. Stack, *Inorg. Chem.* **2005**, *44*, 2131.
[7] J. Cano, G. De Munno, F. Lloret, M. Julve, *Inorg. Chem.* **2000**, *39*, 1611.
[8] I. Muga, J. M. Gutierrez-Zorrilla, A. Luque, P. Roman, F. Lloret, *Inorg. Chem.* **1997**, *36*, 743.
[9] A. Escuer, I. Castro, F. Mautner, M. S. El Fallah, R. Vicente, *Inorg. Chem.* **1997**, *36*, 4633.
[10] V. V. Pavlishchuk, S. V. Kolotilov, A. W. Addison, M. J. Prushan, R. J. Butcher, L. K. Thompson, *Inorg. Chem.* **1999**, *38*, 1759.
[11] A. Escuer, R. Vicente, S. B. Kumar, X. Solans, M. Font-Bardia, A. Caneschi, *Inorg. Chem.* **1996**, *35*, 3094.
[12] Escuer, M. S. El Fallah, S. B. Kumar, F. Mautner, R. Vicente, *Polyhedron* **1999**, *18*, 377.
[13] P. Kopel, Z. Trávníček, L. Kvítek, R. Panchártková, M. Biler, J. Marek, M. Nádvorník, *Polyhedron* **1999**, *18*, 1779.
[14] P. Kopel, Z. Trávníček, L. Kvítek, Z. Černošek, G. Wrzeszcz, J. Marek, *J. Coord. Chem.* **2003**, *56*, 1.
[15] P. Kopel, Z. Trávníček, R. Panchártková, M. Biler, J. Marek, *Transition Met. Chem.* **1999**, *24*, 239.
[16] P. Kopel, Z. Trávníček, R. Panchártková, Z. Šindelář, J. Marek, *J. Coord. Chem.* **1998**, *44*, 205.
[17] P. Kopel, Z. Trávníček, L. Kvítek, M. Biler, M. Pavlíček, Z. Šindelář, J. Marek, *Transition Met. Chem.* **2001**, *26*, 282.
[18] K. Yamanari, Y. Kushi, M. Yamamoto, A. Fuyuhiro, S. Kaizaki, T. Kawamoto, Y. Kushi, *J. Chem. Soc., Dalton Trans.* **1993**, 3715.
[19] W. J. Hunks, M. C. Jennings, R. J. Puddephatt, *Inorg. Chem.* **1999**, *38*, 5930.
[20] F. Cecconi, C. A. Ghilardi, S. Midollini, A. Orlandini, *J. Organomet. Chem.* **2002**, *645*, 101.
[21] I. Haiduc, M. F. Mahon, K. C. Molloy, M. M. Venter, *J. Organomet. Chem.* **2001**, *627*, 6.
[22] S. Kar, B. Pradhan, R. K. Sinha, T. Kundu, P. Kodgire, K. K. Rao, V. D. Puranik, G. K. Lahiri, *Dalton Trans.* **2004**, 1752.
[23] J. Pouchert, *The Aldrich Library of Infrared Spectra*, 3rd ed., Aldrich Chemical Company, Milwaukee, Wisconsin, **1981**.
[24] P. Kopel, Z. Trávníček, R. Zbořil, J. Marek, *Polyhedron* **2004**, *23*, 2193.
[25] M. Ciampolini, *Inorg. Chem.* **1966**, *5*, 35.
[26] A. B. P. Lever, *Inorganic Electronic Spectroscopy*, Elsevier, Amsterdam, **1984**.
[27] W. Addison, T. N. Rao, J. Reedijk, J. V. Rijin, G. C. Verchoor, *J. Chem. Soc., Dalton Trans.* **1984**, 1349.
[28] R. Boča, Program Polymagnet-06. Slovak Technical University, Bratislava, **2006**.
[29] R. Boča, *Theoretical Foundations of Molecular Magnetism*, Elsevier, Amsterdam, **1999**.
[30] R. Boča, *Struct. Bonding (Berlin)* **2006**, *117*, 1.
[31] R. Boča, *Coord. Chem. Rev.* **2004**, *248*, 757.
[32] M. Hitzfed, P. Ziemann, W. Buckel, H. Claus, *Phys. Rev. B: Condens. Matter* **1984**, *29*, 5023.
[33] P. Kopel, Š. Čermáková, K. Doležal, B. Kalińska, A. Bieńko, J. Mroziński, *Pol. J. Chem.* **2007**, *81*, 327.
[34] T. Glaser, M. Heidemeier, S. Grimme, E. Bill, *Inorg. Chem.* **2004**, *43*, 5192.
[35] *SMART and SAINT: Area Detector Control and Integration Software*, Bruker AXS Inc., Madison, WI, USA, **2003**.
[36] G. M. Sheldrick, *SADABS: Program for Empirical Absorption Correction for Area Detectors*, version 2.10, University of Göttingen, Germany, **2003**.
[37] *SHELXTL: Structure Determination Programs*, version 6.12, Bruker AXS Inc., Madison, WI, USA, **2001**.
[38] K. Brandenburg, *DIAMOND: Crystal and Molecular Structure Visualization*, version 3.1b, Crystal Impact GbR, Bonn, Germany, **2006**.
[39] K. Binder, A. P. Young, *Rev. Mod. Phys.* **1986**, *58*, 801.
[40] J. A. Mydosh, *Spin glasses: an experimental introduction*, Taylor and Francis, Ltd., London, **1993**.
[41] D. Gatteschi, R. Sessoli, J. Villain, *Molecular Nanomagnets*, Oxford University Press, **2006**.

Received: July 1, 2009
Published Online: October 29, 2009

